Ion acceleration with ultra-thin foils using elliptically polarized laser pulses

2008 New J. Phys. 10 113005

(http://iopscience.iop.org/1367-2630/10/11/113005)

New Journal of Physics
The open-access journal for physics

Ion acceleration with ultra-thin foils using elliptically polarized laser pulses

S G Rykovanov[1,2,6], J Schreiber[1,3,4], J Meyer-ter-Vehn[1], C Bellei[3], A Henig[1,4], H C Wu[1] and M Geissler[5]

[1] Max-Planck Institute für Quantenoptik, Hans-Kopfermann strasse 1, 85748, Garching, Germany
[2] Moscow Physics Engineering Institute, Kashirskoe shosse 31, 115409 Moscow, Russia
[3] Blackett Laboratory, Imperial College of Science, Technology and Medicine, Prince Consort Road, London SW7 2BZ, UK
[4] Department für Physik, Ludwig-Maximilians-Universität München, Am Coulombwall 1, 85748 Garching, Germany
[5] Department of Physics and Astronomy, Queen's University, Belfast, BT7 1NN, UK
E-mail: sergey.rykovanov@mpq.mpg.de

New Journal of Physics **10** (2008) 113005 (10pp)
Received 27 August 2008
Published 7 November 2008
Online at http://www.njp.org/
doi:10.1088/1367-2630/10/11/113005

Abstract. We present theoretical considerations on the process of ion acceleration with ultra-thin foils irradiated by elliptically polarized, highly intense laser pulses. Very recently the radiation pressure acceleration regime was predicted where mono-energetic ion bunches can be produced with high efficiencies (Klimo *et al* 2008 *Phys. Rev. ST Accel. Beams* **11** 031301; Robinson *et al* 2008 *New J. Phys.* **10** 013021). We have studied the process by means of 1D particle-in-cell (PIC) simulations and analytical models and have considered effects of areal mass density of the target and laser ellipticity on the ion acceleration process. For certain target densities and laser parameters the optimum target thickness has been extracted. Peaked ion spectra are found for ellipticity beyond a threshold value of about 0.7. Here, we highlight the drastic difference between linear and circular polarization by movie animations.

[6] Author to whom any correspondence should be addressed.

Contents

1. Introduction

The acceleration of ions with ultra-high intensity laser pulses has attracted broad interest over the last decade. The high quality of the produced multi-MeV ion bunches in terms of very small values for the transversal and longitudinal emittances has stimulated discussions about a number of applications, such as cancer therapy [1]–[4], isotope production [5, 6], plasma radiography [7], inertial confinement fusion (ICF) [8, 9] etc. However, only within recent years did it become possible to produce mono-energetic ion beams directly from the irradiated targets [10]–[12] which is essential for some of the aforementioned applications. Since the mono-energetic ion beams are still generated via target normal sheath acceleration (TNSA) [13], they suffer from a low laser–ion energy conversion efficiency of usually less than a few percent. Just recently, a new technique for a very efficient generation of quasi-mono-energetic ion beams was proposed by several authors [14]–[18] and also studied experimentally [19]. The key-point is the use of ultra-thin foils and high-contrast, circularly polarized laser pulses. In this paper, we study this new ion acceleration process and consider the effect of the target thickness and elliptical, rather than perfect circular, polarization on the acceleration process by means of one-dimensional particle-in-cell (1D PIC) simulations.

The paper is organized as follows: first we review the concept of ion acceleration in the radiation pressure regime, then we introduce the model equations, and finally present simulations results and discussion.

2. Ion acceleration in the radiation pressure regime

A prominent feature of relativistic laser–matter interaction is that the electrons do not only oscillate in the transverse electric field, but are also pushed longitudinally by the $\mathbf{v} \times \mathbf{B}$ part of the Lorentz force. Thus, focusing an intense laser pulse onto a solid target results in charge separation fields at the front side of the target. Those fields in turn accelerate ions in the laser propagation direction. For linearly polarized laser pulses this front-side acceleration process was studied both theoretically [20]–[22] and experimentally [10, 11, 23] during the last few years. The role of circularly polarized light in high-intensity laser–solid interactions was addressed in recent publications by Macchi *et al* [17] and Liseikina and Macchi [24]. In the case of circular

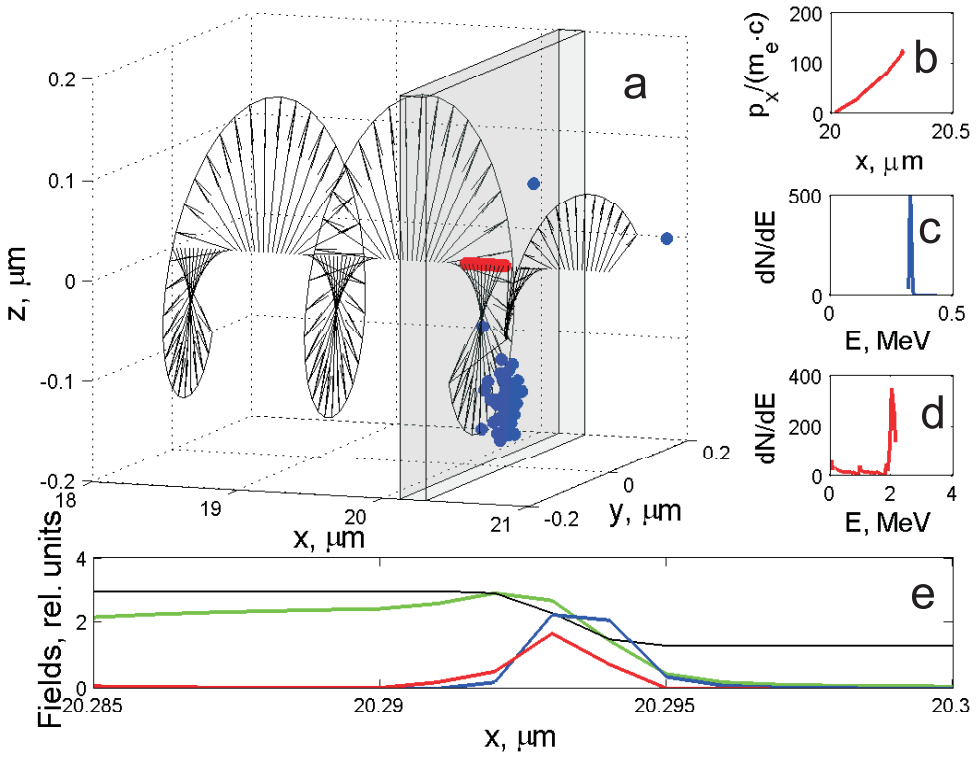

Figure 1. Snapshot of laser–foil interaction taken at the time when the pulse maximum reaches the target. The circular polarized laser pulse is incident from the left. The simulation parameters are: laser amplitude $a_0 = 3$, laser FWHM duration is 15 cycles, target density $n_e = 100 n_{cr}$, and target thickness $l = 0.01\lambda_L$ (the units are explained later in the text). (a) Positions of electrons (blue circles) and ions (red circles) are plotted on three axes in microns as well as electric field (black arrows) in arbitrary units. The transparent box indicates target position. (b) Ion longitudinal ion phase space, (c) electron and (d) ion energy spectra, (e) square root of laser intensity (black), longitudinal field (green), and normalized electron (blue) and ion (red) density.

polarization, the force due to the light pressure, i.e. the $\mathbf{v} \times \mathbf{B}$ term in the Lorentz-force, has no oscillating term and thus leads to less heating of electrons than linear polarization. While electrons are adiabatically pushed into the target, ions can be effectively accelerated in the non-oscillating charge separation field.

The difference between circular and linear polarizations can be traced from animations made from simulation data. We use the 1D3P PIC code PICWIG [25] (the simulations and parameters are described below in section 4), where 1D3P means that each quantity depends only on one spatial coordinate (in our case the x-direction in which the laser propagates), but particles have all three momentum components and generate currents in three dimensions. In order to visualize particle motion in 3D space in figure 1, we select electrons (blue) and ions (red) along the $y = z = 0$ axis, obtain their trajectories by integrating their momenta, and plot them in full 3D space. Figure 1 displays a snapshot taken at the time when the pulse maximum reaches the target. Black arrows represent the electromagnetic fields for a circularly polarized

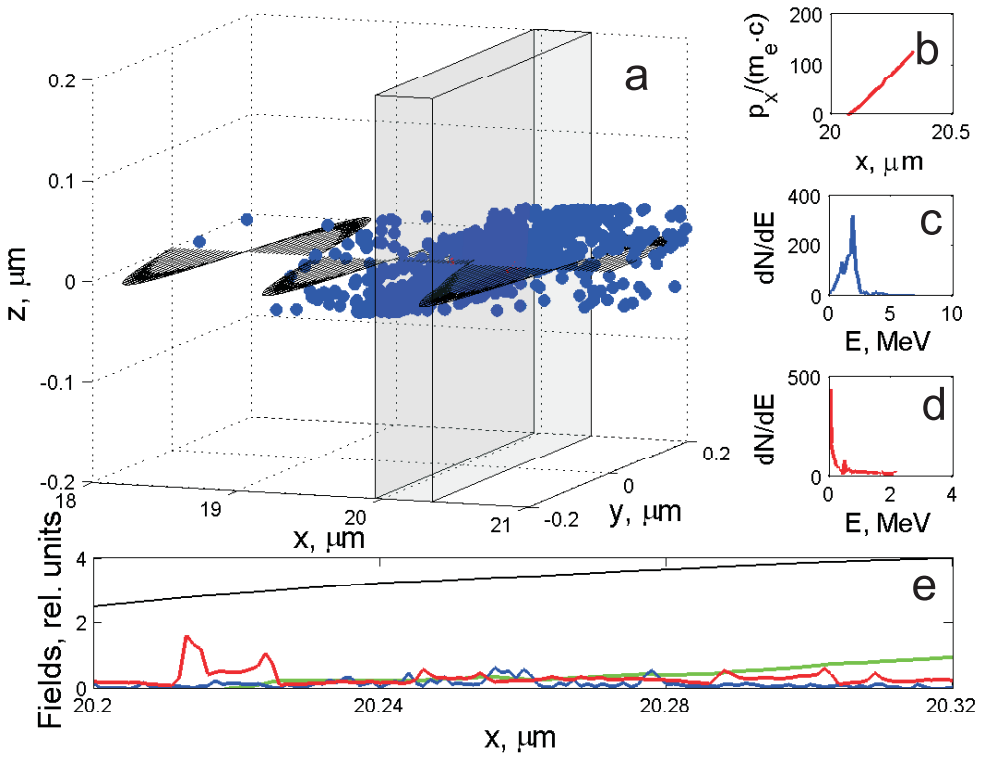

Figure 2. Same as figure 1, but for a linear polarized laser pulse with amplitude $a_0 = 3 \cdot \sqrt{2}$ incident from the left.

laser beam incident from the left side. The target foil is initially located at $x = 20\,\mu$m, and its thickness is 0.01 μm. Figure 1(b) represents the ion phase-space (longitudinal momentum versus ion position). Figures 1(c) and (d) give the electron and ion energy spectra, respectively. Figure 1(e) shows the square root of intensity (throughout the paper by this term we mean the instantaneous intensity) of the laser pulse (black), the longitudinal field (green) and electron and ion densities (blue and red, respectively).

In the case of circular polarization (movie 1, available from stacks.iop.org/NJP/10/113005/mmedia, and figure 1), the longitudinal charge-separation field, that accelerates the ions, is non-oscillating and produces a mono-energetic ion bunch. Electrons are moving in circular orbits and the electron spectrum also exhibits mono-energetic features during the interaction time. After the laser pulse, electron energy decreases because of energy transfer to the remaining foil. It is interesting to notice that in this particular case the longitudinal electric field amplitude becomes as large as that of the incoming laser pulse (see section 2).

The case of linear polarization (movie 2, available from stacks.iop.org/NJP/10/113005/mmedia, and figure 2) is quite different. In sharp contrast to the case of circular polarization, the oscillating component of the laser $\mathbf{v} \times \mathbf{B}$ force drives the electrons into chaotic longitudinal motion back and forth through the thin target foil. This strongly heats the electrons and leads to foil explosion rather than smooth localized ion acceleration. Notice the wide spatial spreading of the longitudinal electric field (green), which accelerates the ions. As a result, we observe broad distributions of electrons (blue) and ions (red) with thermal-like spectra and strongly reduced energy transfer to ions. This confirms the results of three recent publications [14]–[16] that the

use of ultra-thin foils combined with circular polarization of the laser pulse allows for highly efficient generation of mono-energetic ion beam bunches.

3. Model equations

For the following considerations, we assume a steady state of the interaction where the electrostatic pressure is balanced by the radiation pressure of the laser (see also movie 1, available from stacks.iop.org/NJP/10/113005/mmedia). The charge separation field produced by displacing the electron slab with thickness l into the target is given by

$$a_{\mathrm{es}} = Znl, \tag{1}$$

where a_{es} is the electrostatic charge separation field, Z and n are the mean charge state and the density of the target ions, respectively, and l is the thickness of the electron depletion layer [14]. We work in *relativistic units*. The normalized quantities for electric field a, time t, length l, momentum p and density n are obtained from their counterparts in SI-units E, t', l', p' and n' via

$$a = \frac{eE}{m_{\mathrm{e}} c \omega_{\mathrm{L}}}, \quad t = \omega_{\mathrm{L}} t', \quad l = \frac{\omega_{\mathrm{L}}}{c} l', \quad p = \frac{p'}{m_{\mathrm{e}} c}, \quad n = \frac{n'}{n_{\mathrm{cr}}}. \tag{2}$$

Here e and m_{e} are the charge and the mass of the electron, ω_{L} is the laser angular frequency, c is the speed of light in vacuum and $n_{\mathrm{cr}} = \varepsilon_0 m_{\mathrm{e}} \omega_{\mathrm{L}}^2 / e^2$ is the electron critical density. The length of the depletion layer can be found from the balance between electrostatic and radiation pressure, i.e.

$$\tfrac{1}{2} a_{\mathrm{es}}^2 = (1 + R - T) a_0^2, \tag{3}$$

where R and T are the reflectivity and transmission of the foil, respectively. By combining equations (1) and (3) and considering a target of thickness d we introduce the dimensionless parameter

$$\xi = \frac{Znd}{a_0 \cdot \sqrt{2(1 + R - T)}}. \tag{4}$$

The dimensionless parameter ξ defines the regime of interaction. When $\xi = 1$, then the laser pressure is just sufficient to displace all electrons by the target thickness, i.e. the target thickness equals the length of the depletion layer. For $\xi \lesssim 1$, the laser pressure is stronger than the electrostatic pressure, and the electrons are pushed out of the target foil, whereas for $\xi \gtrsim 1$ compressed electrons and space charge field remain inside the foil, accelerating the ions layer by layer [14]. For the latter case, the whole foil is set into motion after the shock launched by the laser front reaches the rear side of the target. In the following, we divide our analysis into two different scenarios: (i) the electrons are completely separated from the foil ($\xi \lesssim 1$), and (ii) the electrons remain bound to the target ions ($\xi \gtrsim 1$).

(i) When the electrons are separated from the foil, the maximum field at the rear side of the target is defined by equation (1), where l must be replaced by the target thickness d. In our 1D consideration, this field is maintained for the duration of the laser pulse t_{L}, which in the nonrelativistic description yields the maximum ion kinetic energy of

$$E_{\xi \lesssim 1} = \frac{1}{2 m_{\mathrm{i}}} \left(Z^2 n d t_{\mathrm{L}} \right)^2, \tag{5}$$

where m_{i} is the mass of the target ions in units of electron mass m_{e}.

In reality, the energy will be less when the 1D description breaks down, i.e. when the separation distance L_s approaches the diameter of the laser focal spot $2r_L$. This would lead to a lower ion energy in equation (5) and may be described by replacing the laser pulse duration t_L by the value $2r_L/c$; here the electrons are assumed to move with speed of light away from the ions given them a shorter time, i.e. $2r_L/c$ to respond on the charge separation fields.

(ii) For $\xi \gtrsim 1$, we assume that the foil remains in its initial shape, and the laser pulse is totally reflected by the target ($R = 1$, $T = 0$ in equation (3)). Then the foil is accelerated by the light pressure, and the equation of motion reads [15, 26, 27]

$$\frac{\mathrm{d}p}{\mathrm{d}t} = Z\frac{a_0}{\xi}\frac{\sqrt{1+p^2}-p}{\sqrt{1+p^2}+p}, \tag{6}$$

where p is the momentum of a single ion of the foil. In the nonrelativistic approximation, the corresponding kinetic energy of the ion is given by

$$E_{\xi\gtrsim 1} = \frac{1}{2m_i}\left(\frac{Za_0t_L}{\xi}\right)^2. \tag{7}$$

It is worth noting that the motion of the foil becomes relativistic, when the momentum $p = Za_0t_L/\xi$ equals 1. For $\xi = 1$ and $t_L = 2\pi$ (single laser cycle), these conditions mark the transition to the laser piston acceleration regime as discussed by Esirkepov *et al* [26]. The corresponding laser amplitude $a_0^{LP} = m_i/(2\pi) = 1836/(2\pi)$ is equivalent to an intensity of 7×10^{23} W cm^{-2} at 1 μm wavelength for a hydrogen target.

Comparing equations (5) and (7) it is evident that they are identical for $a_0 = Znd$ which is similar to the ad hoc definition given in equation (4). Therefore, the ion energy expected for optimal conditions can be approximated by

$$E_{opt} = \left(\sqrt{(Za_0t_L)^2 + m_i^2} - m_i\right), \tag{8}$$

which is the relativistic analogy to equation (5).

4. Simulations

4.1. Optimal conditions for ion acceleration

We have conducted this study using the 1D3P PIC code PICWIG [25]. In planar geometry, it allows to simulate the interaction of intense laser pulses with pre-ionized non-collisional plasma. The plasma density used throughout the paper is $100n_{cr}$ and was chosen to be lower than solid state densities. This is for the sake of simplicity in order to study the basic properties of the ion acceleration with thin foils. The results of this study can be scaled to real densities. The spatial step is equal to 0.5 nm, each plasma cell is initially occupied by 400 macro-particles of each kind (electrons and ions). The ions in this study are assumed to be protons. The laser pulse has a Gaussian envelope, and its duration is the FWHM-value of the electric field envelope. Throughout the paper the duration of the laser pulse is chosen to be 15 cycles, corresponding to approximately 40 fs for $\lambda_L = 800$ nm. In all simulations presented in this work, the density

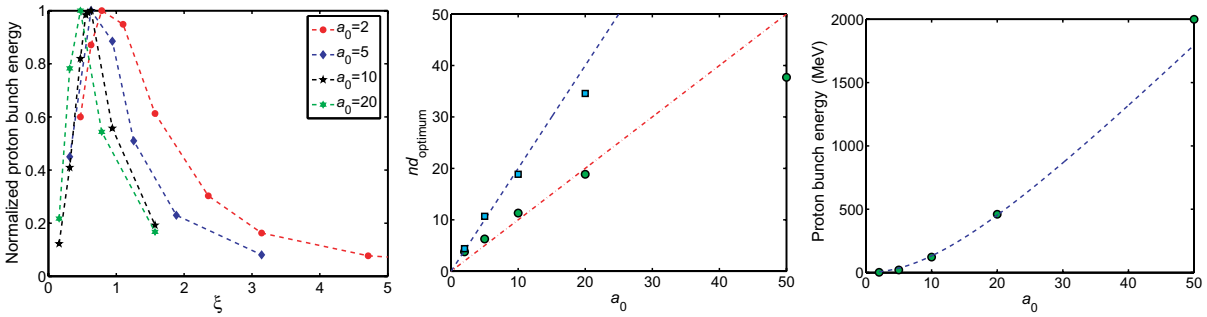

(a) (b) (c)

Figure 3. Results of 1D PIC simulations. (a) Proton bunch energy versus the parameter ξ for different laser amplitudes a_0. (b) Dependence of the optimum mass-density $(nd)_{\mathrm{opt}}$ on a_0 for a laser pulse with Gaussian envelope (circles) and for a flat-top pulse (squares); the dashed and dashed–dotted lines correspond to $(nd)_{\mathrm{opt}} = a_0$ and $(nd)_{\mathrm{opt}} = 2a_0$, respectively. (c) Dependence of ion bunch energy on a_0 obtained from simulation (circles) and from equation (5) (dashed line).

gradient scale length at the plasma–vacuum interface was taken to be zero, i.e. the laser pulse interacts with step-like density profile.

The transition between the regimes $\xi \lesssim 1$ and $\xi \gtrsim 1$ is apparent in figure 3(a), where the proton energy is plotted versus the parameter ξ (equation (4)) for different laser pulse amplitudes a_0. For simple illustrative reasons, we have set $\xi = \xi(R = 1, T = 0)$, implying full reflection and zero transmission. This is actually not true for the thin foils considered here, where transmission is significant, as we saw in figures 1 and 2. Nevertheless, we find from 1D simulations that peak proton bunch energy occurs for $\xi \approx 1$, almost independent of laser amplitude. The important message is then that the optimum foil thickness $(nd)_{\mathrm{opt}}$ scales linearly with laser amplitude a_0. Plotting both quantities from simulations for Gaussian-shaped pulses in figure 3(b), we find indeed proportionality

$$(nd)_{\mathrm{opt}} \approx a_0, \tag{9}$$

given by the dashed line in the important range of $1 < a_0 < 20$. Also for other pulse shapes, the relation $(nd)_{\mathrm{opt}} \approx f a_0$ remains valid, but with different proportionality factor f, for example, we obtain $f \approx 2$ for a flat-top laser pulse. Deviations show up at larger a_0. Those are probably due to the highly simplified derivation of the threshold for complete electron separation. For large values of a_0 the response of the ions to the growing longitudinal electrostatic field cannot be neglected anymore and should be taken into account in the pressure balance equation (equation (3)). With this respect, the motion of the ions becomes important when they approach the speed of light within the initial separation case, which is likely to happen for the case $a_0 = 50$ (figures 3(b) and (c)).

Finally, figure 3(c) shows the ion bunch energy versus a_0 obtained from simulations (circles) and from equation (8) (dashed line) setting $\xi = 1$. It is visible that the ion bunch energy grows proportionally to a_0^2 (equation (7)) and therefore to the laser pulse energy as long as the ion motion is non-relativistic.

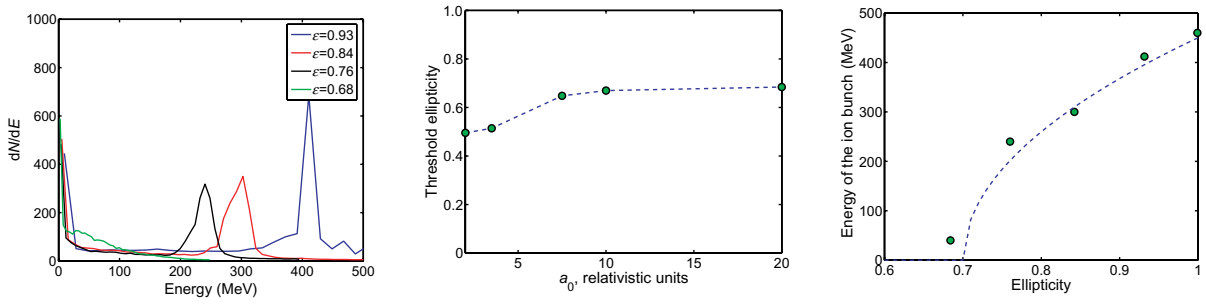

(a) (b) (c)

Figure 4. (a) Proton energy spectra for $a_0 = 20$ and different ellipticities. (b) Dependence of threshold ellipticity on a_0. (c) Dependence of the proton bunch energy on ellipticity for $a_0 = 20$. Beam parameters are the same as for figure 3.

4.2. Ellipticity effects

Suppression of pre-pulses, which tend to degrade density profiles of targets before the main pulse arrives, is required in many experiments. Plasma mirrors have been successfully used in this case to achieve high contrast laser pulses [28, 29]. In the context of the present paper, however, pulses are needed having both high contrast and circular polarization. The problem then is that plasma mirrors will change the polarization of obliquely incident pulses from circular to elliptical, because the p-polarized component is absorbed more strongly than the s-polarized one. Since the plasma-mirrors are often used after the main focusing optics of the laser system, i.e. shortly before target interaction, their effect on the polarization needs to be controlled.

Motivated by this experimental problem, we have studied how the generation of mono-energetic ion beams degrades with decreasing ellipticity and what is the minimum value. Here we define ellipticity as the ratio between the two field components $\epsilon = E_y/E_z$, supposing that the phase difference between them is equal to $\pi/2$ and that $E_y < E_z$. Results are shown in figure 4. Figure 4(a) exhibits ion energy spectra for $a_0 = 20$ and decreasing values of ellipticity. One can see that energies and strengths of spectral peaks diminish with decreasing ellipticity and disappear for $\epsilon < 0.7$. In figure 4(b), the dependence of the threshold ellipticity on laser amplitude a_0 is plotted. For each a_0 the thickness of the target was chosen to be optimal according to the results of the previous subsection. One observes that the threshold ellipticity of $\epsilon \approx 0.7$ is almost independent of a_0, though it slightly falls for $a_0 < 7$. We attribute this latter tendency to reduced electron heating at lower laser amplitudes.

Finally, figure 3(c) shows the dependence of the energy of the ion bunch on ellipticity for $a_0 = 20$. The ellipticity is shown in the range from ϵ_{thr} to $\epsilon = 1$ (circular polarization). The results on peak ion energy can be approximately described by the relation

$$E_{\text{ion}} = E_{\text{circ}}\sqrt{(\epsilon - \epsilon_{\text{thr}})/(1 - \epsilon_{\text{thr}})}, \tag{10}$$

where E_{circ} is the peak ion energy for circular polarization and $\epsilon_{\text{thr}} \approx 0.7$ the threshold ellipticity.

5. Discussion and conclusions

The present study is restricted to 1D analysis and simulation. Multi-dimensional effects have been discussed by Klimo *et al* [14], in particular lateral decay of the ion bunch which limits the time interval available for acceleration to $t_m = \sqrt{2\xi\sigma/a_0}$. Here σ denotes the FWHM diameter of a Gaussian radial intensity distribution. The maximum ion energy then follows from equation (7); for SI-units and $\xi \gtrsim 1$, we find $E_m = (4\sqrt{\ln 2}m_i c^2/\xi)\sqrt{P_L/P_{Ri}}$, where the *ion relativistic power unit* $P_{Ri} = 4\pi\varepsilon_0 m_i^2 c^5/(Z^2e^2) = 29.3$ PW for protons. Under optimal conditions ($\xi \sim 1$), this implies proton energies close to 1 GeV for a laser power of around 3 PW.

In conclusion, the present result clarifies two important points: firstly, the areal density optimal for ion acceleration was found to be $(nd)_{opt} \approx a_0$. Secondly, the degradation of peaked ion spectra as a function of ellipticity of the driving laser beam has been investigated. Peaked spectra exist for $\epsilon > 0.7$, and ion energy decreases $\sim \sqrt{\epsilon - 0.7}$. These results are important when using plasma mirrors for high contrast in upcoming experiments.

Circular polarization may be achieved even when using plasma mirrors. For this one has to take into account the different reflection coefficients for s- and p-polarizations and choose the ellipticity of the incoming beam such that it results in circular polarization after reflection. Deviations from complete circular polarization in the range of 10% can be tolerated, but should not exceed 30%.

Acknowledgments

We acknowledge Hartmut Ruhl, Maxim Efremov, Dieter Habs, Manuel Hegelich and Daniel Kiefer for suggestions and fruitful discussions. SR and AH acknowledge financial support from the International Max-Planck Research School on Advanced Photon Science (IMPRS-APS), JS from German Academic Exchange Service (DAAD). HCW thanks for a grant by the Humboldt foundation, and J Meyer-ter-Vehn acknowledges support by the Association EURATOM-Max-Planck-Institut fuer Plasmaphysik. This work was supported by DFG under contract no TR18 and DFG cluster of excellence Munich-Centre for Advanced Photonics.

References

[1] Malka V *et al* 2004 *Med. Phys.* **31** 6 1587–92
[2] Bulanov S V *et al* 2004 *AIP Conf. Proc.* **740** 414–29
[3] Bulanov S S *et al* 2008 *Med. Phys.* **35** 1770–6
[4] Ledingham K W D, Galster W and Sauerbrey R 2007 *Br. J. Radiol.* **80** 855–8
[5] Fritzler S *et al* 2003 *Appl. Phys. Lett.* **83** 15
[6] Levebvre E *et al* 2006 *J. Appl. Phys.* **100** 113308
[7] Mackinnon A J *et al* 2004 *Rev. Sci. Instrum.* **75** 3531
[8] Temporal M, Honrubia J J and Atzeni S 2008 *Phys. Plasmas* **15** 052702
[9] Naumova N M *et al* submitted
[10] Schwoerer H *et al* 2006 *Nature* **439** 445–8
[11] Hegelich B M *et al* 2006 *Nature* **439** 441–4
[12] Ter-Avetisyan S *et al* 2006 *Phys. Rev. Lett.* **96** 145006
[13] Wilks S C *et al* 2001 *Phys. Plasmas* **8** 542–9
[14] Klimo O *et al* 2008 *Phys. Rev. ST Accel. Beams* **11** 031301

[15] Robinson A P L *et al* 2008 *New J. Phys.* **10** 013021
[16] Zhang X *et al* 2007 *Phys. Plasmas* **14** 12
[17] Macchi A *et al* 2005 *Phys. Rev. Lett.* **94** 165003
[18] Yan X Q *et al* 2008 *Phys. Rev. Lett.* **100** 135003
[19] Henig A *et al* in preparation
[20] Sentoku Y *et al* 2003 *Phys. Plasmas* **10** 2009
[21] Wilks S C *et al* 1992 *Phys. Rev. Lett.* **69** 1383
[22] Silva L O *et al* 2004 *Phys. Rev. Lett.* **92** 015002
[23] Fuchs J *et al* 2005 *Phys. Rev. Lett.* **94** 045004
[24] Liseikina T V and Macchi A 2007 *Appl. Phys. Lett.* **91** 171502
[25] Rykovanov S G *et al* 2008 *New J. Phys.* **10** 025025
[26] Esirkepov T *et al* 2004 *Phys. Rev. Lett.* **92** 175003
[27] Marx G 1966 *Nature* **211** 22
[28] Dromey B *et al* 2004 *Rev. Sci. Instrum.* **75** 645
[29] Nomura Y *et al* 2007 *New J. Phys.* **9** 9